High-speed video observation and phase Doppler anemometry measurements of oil break-up in a model engine crankcase

S. Begg*, G. de Sercey, N. Miché and M. Heikal
* Sir Harry Ricardo Laboratories, Centre of Automotive Engineering,
University of Brighton
Brighton, BN2 4GJ, UK

Abstract

A unique experimental study of the characteristics of the liquid phase of oil in a dynamic model engine crankcase was undertaken using non-intrusive optical measurement techniques. The primary objective of the study was to investigate the mechanisms of oil film break-up at the edge of the crankshaft webbing, fed by oil from the main journal bearing. An idealised crankcase model was designed with production engine components and specifications. The crankshaft was rotated by an electric motor, at variable speeds of up to 6,000 pm, within a transparent box. High-speed photographic visualisation revealed the shape of liquid filaments and particles, formed at the edge of the crankshaft web. Three break-up regimes were broadly identified for speeds from idle to 1800, 4200 and 6000 rpm. In each case, the oil particles followed well-known curved trajectories. The first regime was typified by long, twisting ligaments, ejected from the edge along involute-shaped paths. At greater speeds, discrete particles were observed, pinched-off between the ligaments as they became increasingly elongated and distorted. At the highest speeds, a fine aerosol of oil particles filled the crankcase. The particle diameters were measured in three orthogonal planes using phase Doppler Anemometry. The diameters varied in the range of between 2 and 130 µm, depending upon the rotational speed, crank angle and spatial location within the crankcase. The distribution of particle diameters and velocities varied greatly between the measurement planes located in front of and behind the crank web. The maximum mean oil particle velocities recorded were of the order of 25 ms^{-1}. Striations in the droplet arrival time-based data were noted. The autospectral density function showed harmonics of up to 4 times that of the rotational frequency. The droplet formation was considered analogous to a spinning disk atomiser. The variation in the droplet Bond number was evaluated over the limiting range of particle velocity and size and the range of characteristic diameters of the irregular crank web circumference. The disk Bond number, Bo_D was compared to the universal power law for the so-called primary particle size range formed by a spinning disk aerosol generator. The Bo_D and empirical constant, K were estimated at 2.21 and in the range of 1.82 to 2.39 respectively. The windage effect upon the oil in the sump and the film deposited on the crankcase walls were observed at speeds greater than 3000 rpm. A thick, broad, moving film of oil was formed on the upper, inner surface of the crankcase shroud. The oil pool on the surface of the baffle tray was pushed clear of the drainage louvers leading to increased agitation of the surface of the sump oil, funnelling and foaming.

Introduction

The generation of an oil aerosol and the aeration of engine oil occur in the typical operation of an internal combustion engine. As an aerosol, the oil contributes as a source of pollution (and potentially drag) that must be filtered out. When air is trapped in the oil, it has an adverse affect upon the efficiency of the oil to lubricate, cool and actuate engine components and systems. Generally, exhaust gases are also trapped as bubbles in foams or absorbed directly into the working fluid. The greatest affect occurs in the engine crankcase where lubrication is required for the piston and crankshaft. Ejected oil splashes against the oil films deposited on the chamber surfaces. In addition, the rotational and reciprocating motions induce pumping windage of the oil in the baffle tray and wet sump. A comprehensive review can be found in the literature [1-3].

In this study, the break-up process was considered analogous to that of a spinning-disk atomiser. The engine oil, leaking from the crankshaft main bearings, forms a thin film that spreads out over the surface of the rotating crankshaft. A liquid rim is formed at the edge of the spinning-disk. Oil filaments and discrete particles are ejected when the centripetal forces exceed the adhesive and surface tension forces as the speed of rotation is increased [4]. The diameter of the aerosol particles from a rotary atomiser has been shown to be a function of rotational speed and diameter, mass flow rate, surface tension, liquid film wave amplitude [5] and surface topology [6]. Experimental measurements have led to a range of dimensionless terms and empirical constants used to describe the different break-up mechanisms, described as drop-wise break-up, ligament disintegration and sheet break-up [7, 8]. In atomiser studies, the break-up of droplets occurs at regular intervals around the perimeter of a disk of constant radius. In the case of the crankshaft, the shape and thickness of the web, as well as the variation

* Corresponding author: S.M.Begg@brighton.ac.uk

in oil flow rate, implies that several simultaneous modes of break-up can occur and therefore a range of characteristic disk diameters must be proposed.

Experimental Method

An idealised crankshaft test rig was designed for the study. A schematic of the test rig is shown in Fig. 1. It was based upon available production engine crankshaft components. The test rig incorporated an oil pan, baffled windage tray and a modified, balanced, single web crankshaft. The crankshaft was mounted in a bearing block and coupled to a variable speed motor. Surface roughness, mechanical tolerances, and oil type (Castrol Edge Sport 10W60) were carried over from the production engine. Oil temperature and pressure were controlled by an external conditional circuit. The oil temperature was maintained at 75 °C ± 5 °C. The oil pressure was regulated to 6 bar ± 0.2 bar at operating temperature. The mass flow rate of oil to the main crankshaft bearing was measured in situ using a turbine flow meter. The mass flow rate from one side of the crankshaft web for a single bearing was measured between 0.1 and 0.4 $lmin^{-1}$ in the range of 0 to 6000 rpm and 30 to 75 °C. Rotational crankshaft speed was measured using an optical shaft encoder. The crankshaft assembly was mounted within a rectangular case, incorporating glass windows and a modified bearing block, designed maximise the viewing area of the sump and crankshaft from three directions.

Metal curtains (cf. double glazing) were used to minimise the effects of oil fouling upon the windows. A pneumatic piston was used to raise the curtains rapidly prior to the start of the measurement. Within the chamber, a moulded polycarbonate shroud was used to mimic the geometry of the production crankcase and provide optical access to the region directly behind the webbing. The clearance distance between the crankshaft axis and the sump baffle tray and oil surface were carried over from the production engine. The test rig was operated at speeds of up to 100 Hz using a conventional crankcase breather. The origin of start of rotation (0 °CA, top-dead centre) was defined as the position where the nose of the crank web pointed vertically upwards (away from the baffle). Non-intrusive experimental techniques were applied to characterise the dynamic oil behaviour in three key observation planes. The optimisation of these techniques formed an important part of the study. A summary is given in the following section. A review of the techniques is beyond the scope of this paper but can be found elsewhere [e.g. 9]. The origin of the orthogonal axes set *(x, y, z)* for the PDA measurements is denoted by (0, 0, 0) in Fig. 1, 2 and was coincident with the machined front face of the crankshaft web. All measurements were in mm. The axes were defined as follows:

- *x-axis*- along the axis of the crank rotation, positively in the direction away from the motor.
- *y-axis*- along the machined surface of the crank web, positively towards open end of the shroud (*v*, radial component of velocity, denoted as LDA4{2}).
- *z-axis*- along the machined surface of the crank web, positively towards the roof of the rig (*u*, axial component of velocity, denoted as LDA1).

The definition of the measurement planes A, B and C, illustrated in Fig. 2, were as follows:

- *Plane A* – plane parallel to the *x-y* plane through *z = 0*
- *Plane B* – plane parallel to the *y-z* plane through *x = 5*
- *Plane C* – plane parallel to the *y-z* plane through *x =-10*

High-speed ciné photography (HSP) was used to visualise the scattering of oil from the main bearing and crankshaft web. In addition, the formation of liquid films upon the crankcase shroud and windage tray was studied over a range of rotational speeds. A Redlake MotionPro camera and high intensity spotlights were used to record 8-bit ciné sequences at frame rates of up to 100 kHz. The resolution of the images was varied according to the required frame rate.

A Dantec classical, Phase Doppler anemometer (PDA) was used to measure oil particle velocity components and diameters simultaneously at a series of point locations in three orthogonal planes in front of and behind the crank face. A range of forward scatter collection positions were investigated to identify the optimum configuration for each of the measurement planes. The system was set-up to detect forward scattered, *p*-plane polarised light at an angle of 74.5 °. The position of the incident probe and collection optic relative to the crankshaft web were controlled by a precision rectilinear traverse. The control software was programmed with a defined measurement grid. The accuracy in the traverse position is ± 0.1 mm. The specification of the PDA system is given in Table 1.The refractive index, viscosity and density of the oil was measured at 25 °C and 80 °C by an independent laboratory (Intertek, Caleb Brett, ITS Testing Services (UK) Ltd., Essex, UK). Measurements were carried out a 1500, 3000, 4500 and 6000 rpm for comparison. The one pulse per revolution marker (set at 0 °CA) was used to start the PDA measurements. Velocity components were measured as non-coincident data over consecutive cycles using two internal timing clocks. Data was collected for up to 10,000 individual droplet counts in

both the axial and radial directions. However, in certain regions of the crank rig, data acquisition was reduced due to wall-wetting, splashing, non-spherical particles and poor signal to noise ratio. These effects contributed to a poor data validation rate (the ratio of total data acquired to that rejected by the instrument). In these regions, the data validation rate was less than 50%.

Results and Discussion

High-speed visualisation

The mechanism of break-up of the oil into ligaments and particles varied with engine speed. It was characterised by the formation of a film of oil, originating from the main journal bearing. The wrinkling effect induced by the entrained airflow behind the crankshaft upon the oil film surface on the bearing block was also evident. The oil film spread across the surface of the crankshaft webbing. At the edge of the web, the oil separated from the surface, ejected as a series of arc-like (involute) patterns. Three phases could be clearly identified in the high-speed photographs as the rotational frequency was increased. An example of the first phase is shown in Fig. 3 for an engine speed of 1800 rpm. A series of liquid cords (ligaments) remained attached to the trailing edge of the crankshaft web during a rotation until impingement occurred upon the baffle tray or the shroud walls. The formation of the ligaments occurred in sets of between 4 and 8 individual columns. The point of detachment was consistent with the position of the maximum radii, on the front of the crank web and with the positions of change in cross-section, on the rear. The oil was deposited as a thin, narrow film upon the crankshaft shroud.

As the engine speed was increased further, necking of the ligaments was followed by 'pinching-off' of larger diameter, droplet groups. These droplets impacted with the chamber wall and baffle tray. As the speed was increased further, atomisation of the oil occurred at the edge of the web. An oil mist was formed in a series of bands that lagged the leading edge of the crank shaft web as shown in Fig. 4. The oil mist bands were interspersed with regions of low droplet density and large discrete droplets. At the highest speed, identification of high-speed, individual droplets was obscured by the impinging and rebounding oil particles. The chamber was filled with a fine aerosol. The thickness and breadth of the oil film on the shroud wall increased to a maximum at the greatest speed. The film moved across the surface of the chamber surfaces. Large oil droplets formed as drips on the upper chamber surfaces. These were observed to splash onto the tray or the rotating crankshaft. The oil film was cleared of the baffle tray drain louvers by the induced air motion.

The effects of windage were observed in the sump, below the baffle tray level, where the oil is often considered motionless. Air bubbles in the oil could be identified as swirling, lighter coloured layers. The darker coloured oil, largely unmixed, was more opaque. The re-circulating structure filled the depth of the idealised sump at the highest speeds.

The photographic evidence was used to determine the three measurement planes for the PDA investigation.

Oil particle diameter and velocity characteristics

The instantaneous mean oil particle diameter and velocity data were recorded using the PDA technique over a range of crankshaft speeds in two vertical planes and one horizontal plane. The data was processed by standard methods. In the first case, the arrival time-based data, acquired over consecutive cycles, was sorted as velocity and diameter probability density functions. Secondly, ensemble-averaged axial and radial velocity data, as well as particle diameter, were calculated in a series of equal time bins at each location. The moments were used to construct spatial plots within the three planes. The spatial plots showed that the particle size and velocity distributions varied greatly between the front and rear of the crankshaft face. Finally, spectral analysis of the velocity data was performed, when the data rate and sampling interval were suitable, to identify the frequency of the structures identified in the visualisation study.

A typical time series of instantaneous radial (*v*, *LDA4*) particle velocity recorded over consecutive cycles is shown in Fig. 5, redistributed over one rotation, at 6000 rpm. The location (denoted by a cross in Fig. 4) was chosen to for the relatively high data rate and to illustrate the particle spray cloud observations in Fig. 4. The position was in the *y*-*z* plane at x = 10 mm (behind the front surface. It can be seen from the plot that the arrival of oil particles at the measurement location did not occur as continuous data but in batches. In particular, the radial velocity data showed crank angles where striations were observed. The period of the streaks varied with crankshaft speed and spatial location. The corresponding autospectral density function of the radial velocity component data (m^2s^{-1}) is shown in Fig. 6. Sample and hold re-sampling of the data prior to a FFT was carried out up to a maximum frequency of 1 kHz using a sampling frequency of 2048. A prominent peak can be identified at the operating frequency of 100 Hz. Several smaller peaks can be observed at 200 and 300 Hz. The highest frequency occurred at 400 Hz, indicating the passage of up to four sets of particle clouds within one rotation. The spectral response varied at other locations.

In Figs 7 and 8, the ensemble-averaged velocity data are plotted against crank angle for one rotation of the crankshaft in Plane C, behind the crank web face. The two plots illustrate the differences between the axial and radial velocity components and the RMS fluctuation within the sampling timebins. In Fig. 7, the RMS contribution to the axial mean flow component is half the magnitude of the ensemble-averaged velocity. The mean velocity peaks at approximately 100 CA but generally lies between 8 and 14 ms^{-1}, in the upwards direction. In Fig. 8 the RMS component is of comparable magnitude to the ensemble mean radial velocity component over all crank angles suggesting a significant contribution from rebounding droplets. Maxima in the mean radial flow were observed at approximately 150 and 250 CA. The magnitude varied between 2 and 7 ms^{-1}. Generally, the magnitude of the axial and radial particle velocities decreased with increasing y and z. The highest axial velocities were recorded close to the upper portion of the shroud in the range $77 \leq y \leq 83$ mm. The greatest particle mean diameters were recorded in the upper left quadrant of all of the measurement planes. As expected, the ensemble-averaged velocities and diameters increased with an increase in speed. The increased data rate at the higher speeds was offset by the poorer signal to noise ratio.

The disk Bond number

The spinning disk atomiser is a device used to create a monodisperse aerosol of fluid droplets from the edge of a rotating disk that is continuously fed with a liquid supply. The dimensionless Bond number, *Bo* is one of the quantities that can be used to describe the behaviour of a droplet acted upon by a body force with surface tension, σ. In [7], the Bond number was re-defined in terms of a characteristic length scale, *D* determined by the dimensions of the spinning disk, such that:

$$Bo_D = (\rho_l g^* D^2)/4\sigma \quad (1)$$

where ρ is the liquid density and g* is the body force due to the centripetal acceleration. Simpkins ([4]) showed that for a broad range of data (liquid physical properties, flow rates and disk geometries gathered from previous studies, [5, 6]), the dimensionless droplet diameter, (*d/D*) could be represented by a universal power law, where the $0.98 \leq Bo_D \leq 2.3$ and an empirical constant, K that falls in the range of between 2.6 and 7.0. However, in the analysis, a distinction must be made between the primary and satellite particles generated; those that originated from the break-up of the rim film from the disk edge and those generated by secondary atomisation.

In a preliminary analysis, the PDA data was used to infer a distinction between the primary and satellite particles present in the aerosol droplet size distribution with respect to the frequency of rotation and a characteristic crankshaft diameter; the break-away diameter illustrated in Fig. 3. The values of *D* varied between 92 mm and 135 mm. The limits of the range of droplet diameters, *d* was determined from the PDA data at two rotational speeds and for locations in Plane A, B and C. Frequency histograms for velocity and diameters, distributed in 50 bins, are shown in Fig. 9 for 6000 rpm at a location behind the crank web surface (10, -100, 0); Fig. 10, at a location in front of the web (-1-, 100, 0) and in Fig. 11 for the same location but at 3000 rpm. In each case the distributions for droplet velocity and diameter are markedly different. In the 3000 rpm case, in Fig. 11, the droplet diameter range of significance was broad, from approximately 10 - 130 µm. For the 6,000 rpm case, in Fig. 9, the significant range was reduced to between approximately 5 - 70 µm. In Fig. 10, the range was between the two other cases, approximately between 2 and 100 µm; the particle counts were higher due to the improved signal to noise ratio in the less dense region. The diameter ratio, (*d/D*) was plotted against Bo_D, for these limiting conditions. The results are shown in Fig. 12 for the two extreme cases at the limits of the size and speed ranges. The universal power law adopted by [7] is included for comparison as well as the findings of a previous study by [6]. It should be noted that the satellite droplets are considered superfluous in a spinning disk atomiser and are removed. In each case, the closest fit to the power law was achieved for the largest droplets ejected from the crank web. The droplet diameter ratio for these conditions was approximated by the power law of the form:

$$(d/D) = 1.30 Bo_D^{-0.33} \quad (2)$$

This implied that the Bo_D is a constant given by $Bo_D \cong 2.21$. The empirical constant, K was obtained from the general form of the equation for the primary droplet diameter [7]:

$$d = K/\omega \, (\sigma/(\rho_l D))^{1/2} \quad (3)$$

For the recorded measurements, *K* was in the range of 1.89 to 2.39. This was lower than the approximate range of values generally reported in the literature for primary droplets generated by a spinning disk atomiser. It should be noted that it is likely that a moment mean, opposed to a number mean diameter, will provide a better fit to the law and for the analysis of the drag force on the crank or the filtration requirements in the engine breather. As such D_{30}, D_{32} or $Dv_{0.5}$ may be more appropriate equivalent diameters.

Experimental uncertainty

The performance of the PDA system varied considerably with measurement location, velocity bandwidth selection and particle concentration. In particular, the poor signal-to-noise ratio and the requirement for high signal gain and a low validation threshold resulted in the generation of spurious data. This was most evident for positions behind the crankshaft face. At the lower engine speeds, fewer individual particles were recorded, in part, due to the lower oil flow rate, but also due to the unstructured particle shapes. At the higher speeds, the aerosol suspension and the wall films reduced the signal visibility and introduced multiple scattering effects. To minimise the effects, a small probe volume with 8 fringes, low laser power and a large scattering angle were employed. In all cases, it was most difficult to make accurate measurements close to the crankshaft web, although axial velocity validation rates greater than 90% could be achieved at certain locations. In the radial case, the lowest validation rates of approximately 30% were recorded in the upper-left quadrant of the plane directly behind the crankshaft. In this region, the curvature of the shroud played an additional role (to that of the liquid film) in complicating the evaluation of the frequency and phase content in the scattered light signal. Therefore, the data in these regions, although indicative of the phenomena, represent a subset of the population and must be considered with care.

An estimate in the variation of measured Bond numbers was given as ± 40% about the power law in [6] for the different types of liquids, flow rates and disks investigated. If we expect our results to fall within this range, then the estimated error in the Bo_D is ± 0.88.

Conclusions

A phenomenological study of the characteristics of a two-phase oil and air flow was undertaken in an idealised crankshaft case. The study was first introduced by the authors in [10-12]. High-speed visualisation and phase Doppler anemometry were used to observe and measure the processes of oil spray formation from the periphery of the crankshaft web in a manner analogous to a rotary disk atomiser. The results varied with spatial location, throughout an individual rotation, from one cycle to the next and with crankshaft rotational speed (oil flow rate). Large particles were observed to drip from the crankcase surfaces, colliding catastrophically with the crankshaft and oil films. Generally, the characteristics of the oil droplet-laden flow exhibited some steady flow behaviour, in phase with the fundamental and harmonic frequencies of rotation. Unsteady flow characteristics were observed closer to the chamber walls and in the regions of impingement.

Measurements were successfully carried out behind the plane of the machined crankshaft web face and in-line with the main bearing at speeds up to 6,000 rpm. The measurement of the radial velocity component was most affected by the presence of the impinging liquid film. For crankshaft speeds of less than 1,800 rpm, a narrow, thin fuel film was formed on the shroud. Oil was expelled in a discontinuous manner from the edges crankshaft web as a series of sinuous ligaments. At crankshaft speeds between 1,800 and 4,200 rpm, large, discrete particles were observed as well as intermittent spray clouds. At the highest speeds, a fine aerosol of oil particles filled the crankcase. The measured particle diameters varied in the range of between 2 and 130 µm depending upon location within the crankcase. The maximum, mean particle velocities were of the order of 25 ms^{-1}. The frequency of the ejected oil particles varied with the angular position of the crankshaft during a rotation. The distribution of oil particle diameter and velocities varied greatly between the front and rear of the crank web. A thick, broad film of ejected and rebounding particles was formed on the inner surface of the shroud. In addition, oil was driven clear of the surface of the windage tray. Increased aeration of the surface of the sump oil and funnelling were observed.

For the case of the largest individual droplet sizes measured, the ratio of the particle diameter to the characteristic crankshaft web diameter at which oil was observed to ejected, d/D and the disk Bond number, Bo_D compared favourably with the universal power law for the so-called primary particle size distribution generated by a spinning disk atomiser. The Bo_D and range of empirical constant, K were estimated at 2.21 and between 1.89 and 2.39 respectively. However, the universal law had over-predicted the droplet size here and in further work, it is suggested that an evaluation of moment mean or other equivalent diameters is carried out as a better approximation.

Acknowledgements

The authors wish to thank R. Gilchrist of Ricardo UK Ltd and Y. Noda and Y. Mamiya of Nissan Motor Co., Ltd, Japan, for their permission to publish these results. The technical expertise of Messrs. Mr Bill Whitney, Mr Ken Maris and Mr Brian Maggs was very much appreciated.

References

[1] Totten, G., Sun, Y. and Bishop, R. "Hydraulic fluids: foaming, air entrainment and air release – a review," *SAE technical paper 972789* (1997).
[2] Baran, B. and Cheng, W. "Assessing the windage tray blockage effect on aeration in the oil sump," *SAE technical paper 2007-01-4109* (2007).
[3] Manz, D. "High-speed video observation and on-line measurements of oil aeration in an internal combustion engine," MSc Thesis, Massachusetts Institute of Technology (2005).
[4] Matar, O.K., Sisoev, G.M. and Lawrence, C.J., *Chemical Engineering Science* 63:2225-2232 (2008).
[5] Sisoev, G.M., Matar, O.K. and Lawrence, C.J., *J. of Chem. Tech. & Biotech.* 78:2-3 pp.151-155 (2003).
[6] Whitby, K.T., Lundgren, D.A. and Peterson, C.M., *J. Air Wat. Poll.* 9:263-277 (1965).
[7] Simpkins, P.G., *Aerosol Science and Tech.* 26:1, pp.51-54 (1997).
[8] Edelbauer, W., Kratochwill, H., Brenn, G. and Tatschl, R., *Prog. in Computational Fluid Dynamics* 9:1 pp. 1-15 (2009).
[9] Albrecht, H. –E, Borys, M., Damaschke, N. and Tropea, C. *Laser doppler and phase doppler measurement techniques,* Springer, 2003 ISBN 3-450-67838-7.
[10] Begg, S.M., de Sercey, G., Heikal, M.R., Gilchrist, R., Noda, Y. and Mamiya, Y. "Experimental investigation of the characteristics of oil behaviour in an idealised engine crankcase," *Proc. JUMV Intl. Automotive Conf. and Exhibition*, Paper 35 (2009).
[11] Begg, S.M., de Sercey, G. and Heikal, M.R. "Experimental investigation of the characteristics of oil behaviour in an engine crankcase," *Proc. DIPSI Workshop - Droplet impact phenomena and spray investigations.* Universita degli Studi di Bergano, Bergano, Italy, CD (2009).
[12] Begg, S.M., de Sercey, G., Miché, N. D. D., Heikal, M. R., Gilchrist, R., Noda, Y., Tsuruoka, Y. and Mamiya Y. *Submitted to Atomization and Sprays* (2009).

Table 1. Summary of operation of the Dantec classical phase Doppler anemometer

Wavelength	514.5 and 488.0 nm
Focal length	310 mm
Beam diameter	2.2 mm
Beam separation	14 mm
Number of fringes	8
Fringe spacing	5.76 and 5.46 μm
Forward scattering angle	74.5 °
Phase validation range	10 %
Particle refractive index range	1.448 / 1.467 at 80 °C / 25 °C respectively

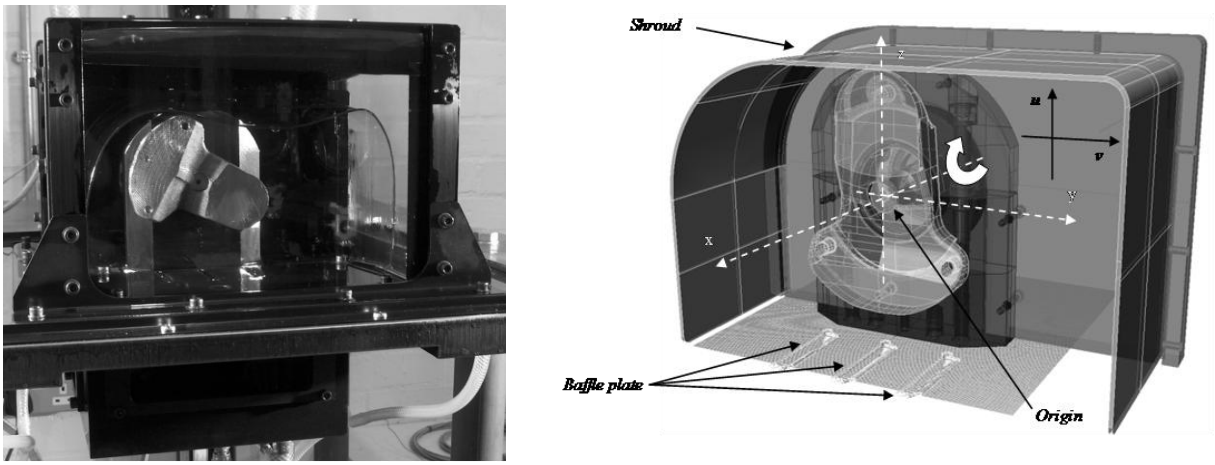

Figure 1. Photograph and schematic of the crank rig and sump showing the sense of rotation and axes convention

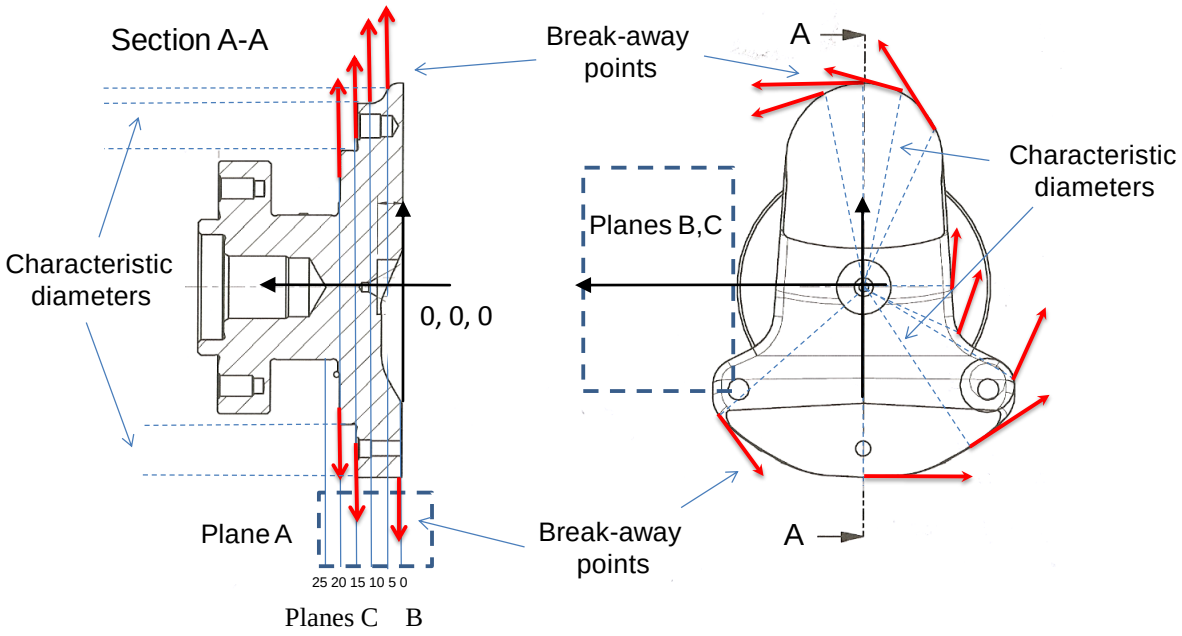

Figure 2. Geometry of crank web showing location of measurement planes and illustration of oil break away points and the definition of the characteristic range of length scales. The range of characteristic diameter, *D* was chosen from the crank web geometry. The range of droplet diameter, d was chosen from the range in values recorded by the PDA in measurement planes A, B, C.

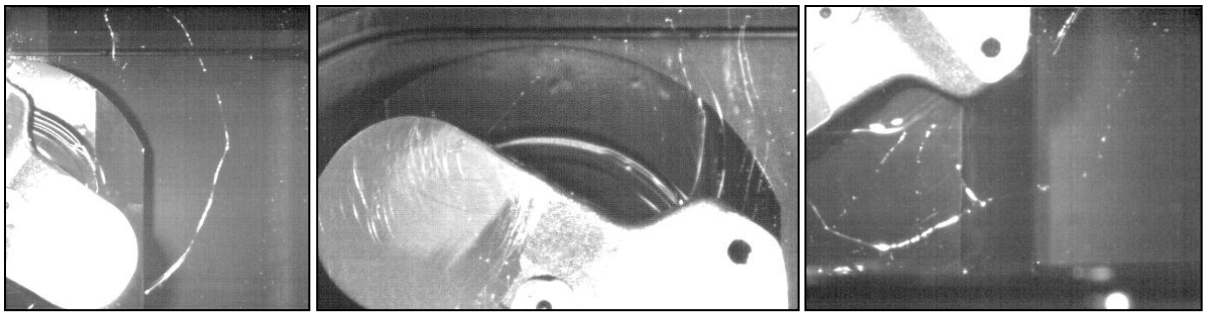

Figure 3. Break-up of oil ligaments at 1800 rpm showing (left to right), leading edge crank nose, multiple sets following the web and baffle plate impingement

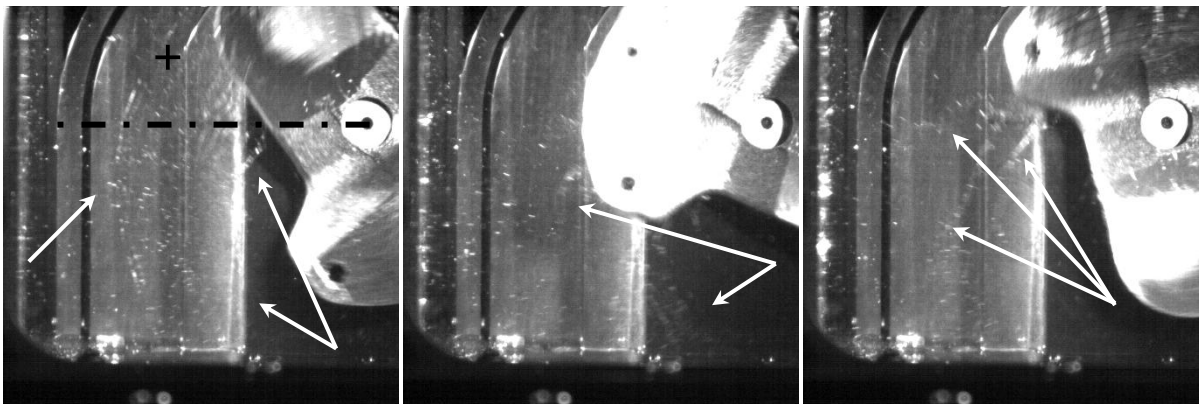

Figure 4. Oil particle spray patterns at 4000 rpm. The arrows indicate the advancing wavefront of the particle cloud band. The measurement location used in the example is marked with '+')

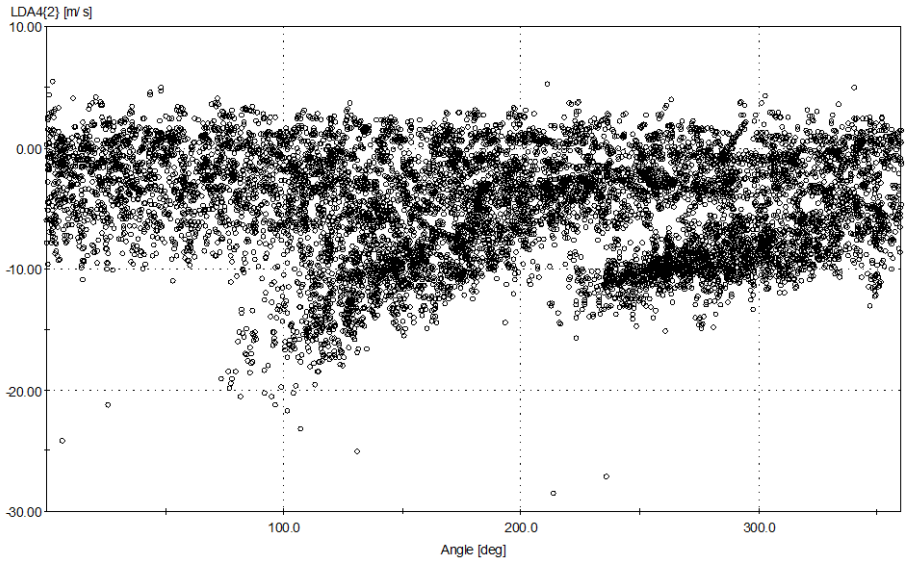

Figure 5. Cycle-resolved, instantaneous radial velocity component with crank angle at 6000 rpm at location 10,-90, 30 in plane C

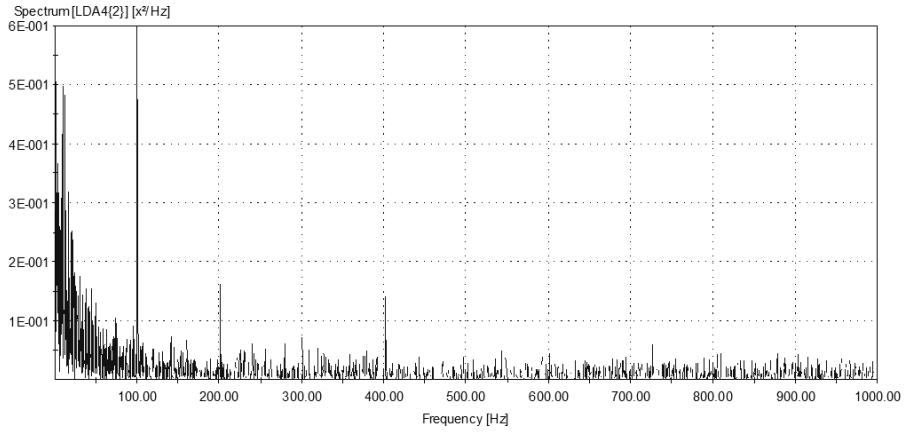

Figure 6. Autospectral density function of the radial velocity component at 6000 rpm at location 10,-90, 30 in plane C

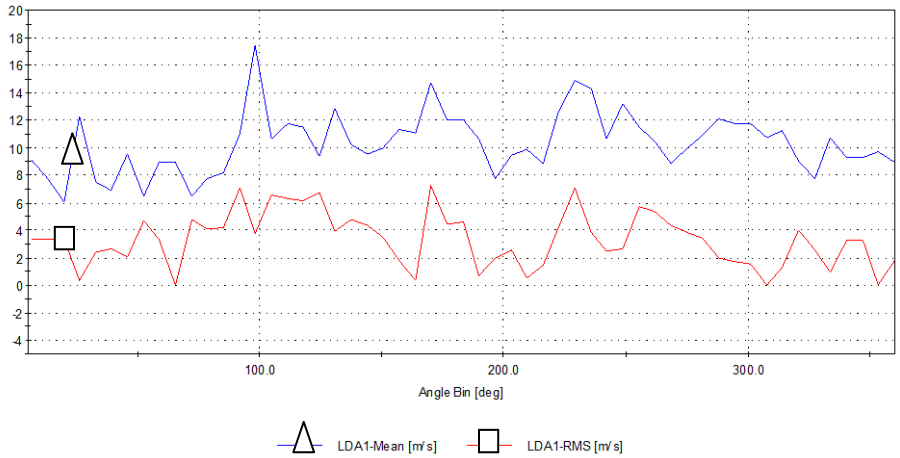

Figure 7. Ensemble-averaged axial velocity component with crank angle at 6000 rpm at location 10,-90, 30 in plane C

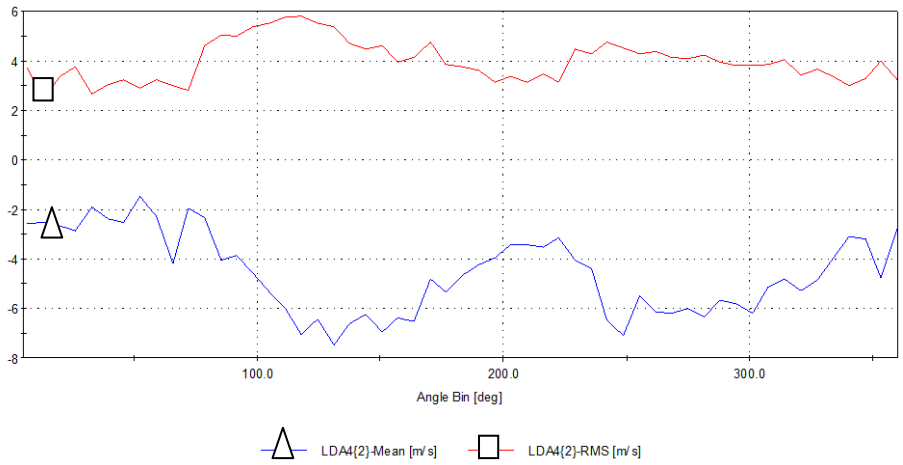

Figure 8. Ensemble-averaged radial velocity component with crank angle at 6000 rpm at location 10,-90, 30 in plane C

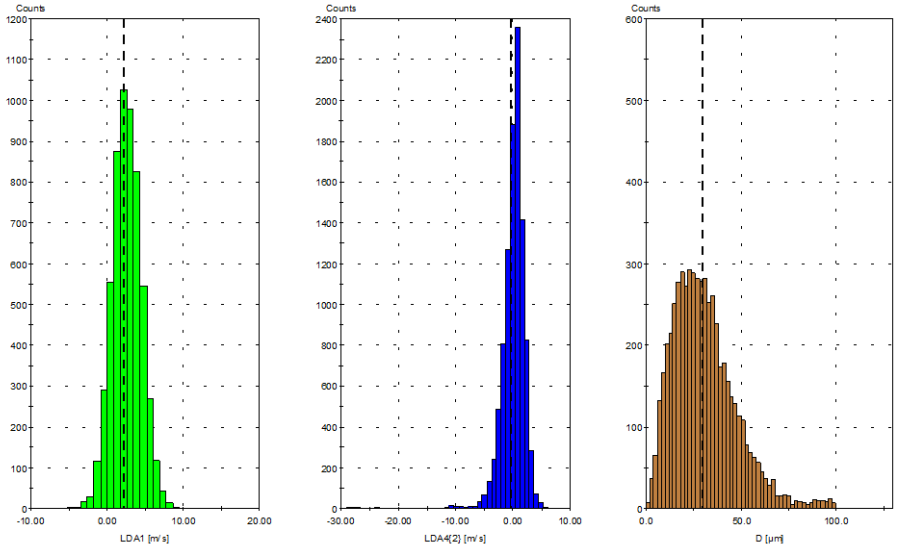

Figure 9. Frequency histograms for axial, radial and droplet diameter at 6000 rpm at location 10,-100, 0 in plane A- rear (dashed line indicates mean value)

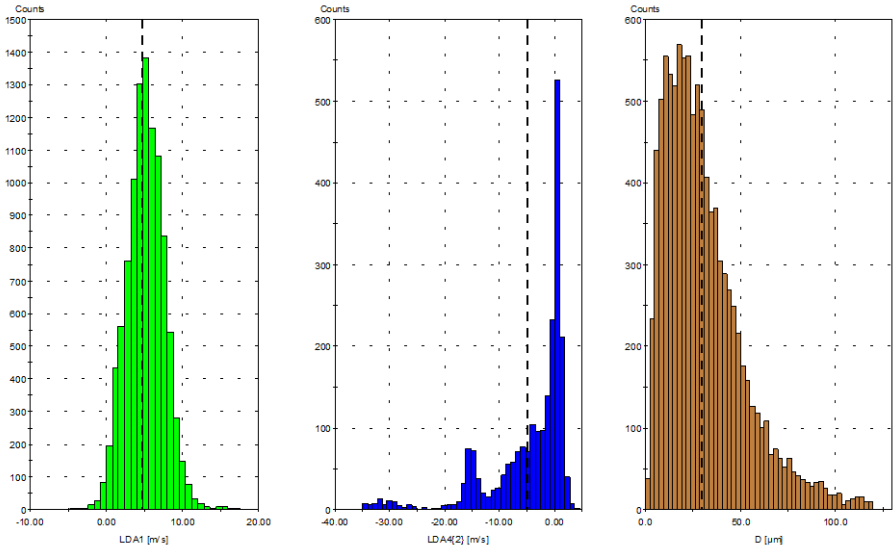

Figure 10. Frequency histograms for axial, radial and droplet diameter at 6000 rpm at location -10,-100, 0 in plane A- front (dashed line indicates mean value)

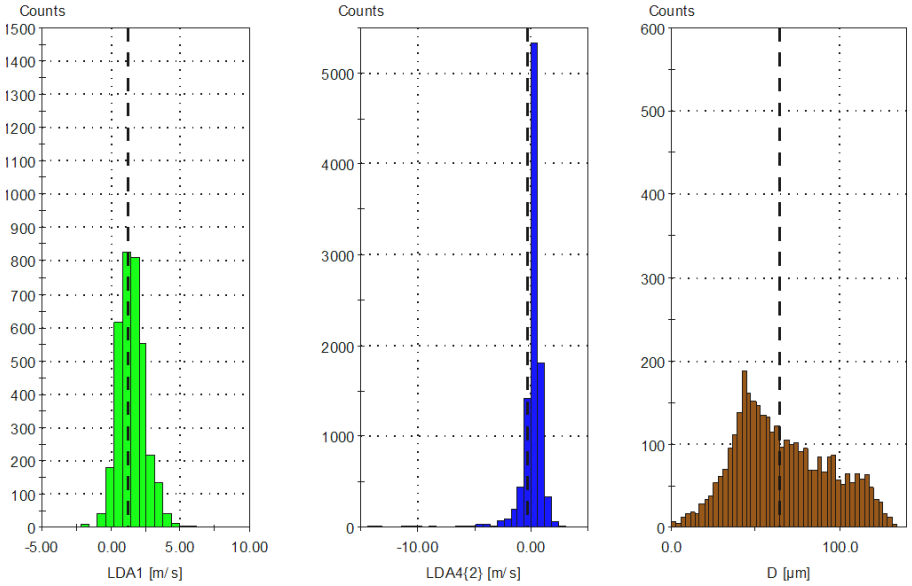

Figure 11. Frequency histograms for axial, radial and droplet diameter at 3000 rpm at location -10,-100, 0 in plane A- front (dashed line indicates mean value)

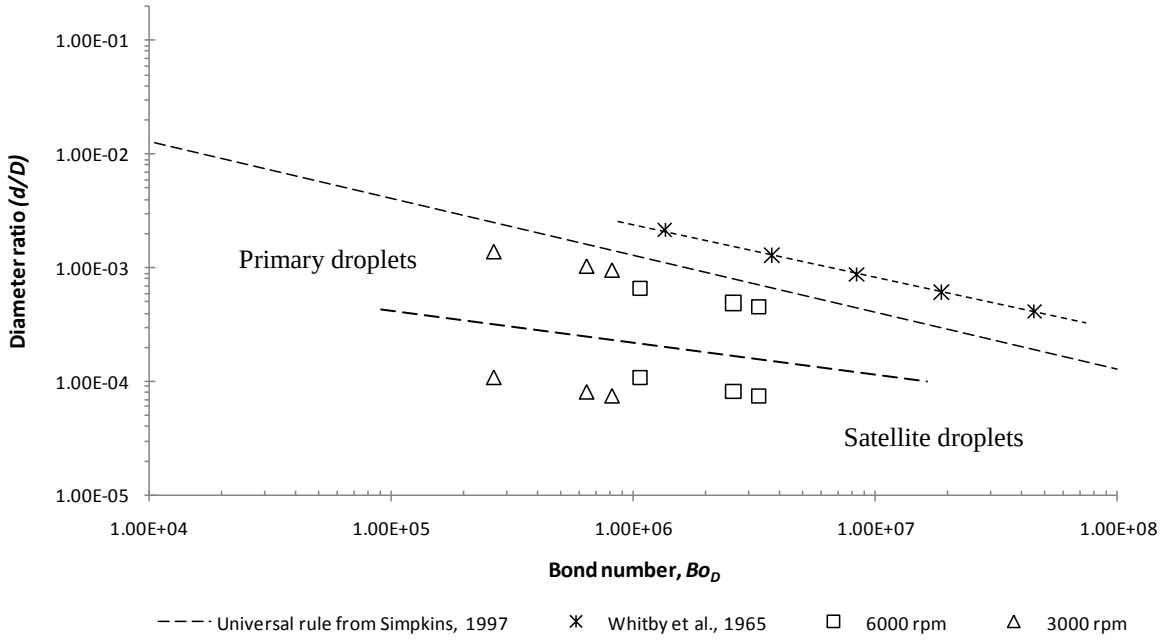

Figure 12. Diameter ratio, (*d/D*) as a function of primary disk Bond number, Bo_D for the range of smallest satellite droplets and the range of the largest, primary droplets at 3000 rpm (Δ) and 6000 rpm (□).